Helmholtz-Zentrum Dresden-Rossendorf (HZDR)

HZDR
HELMHOLTZ ZENTRUM
DRESDEN ROSSENDORF

Point and extended defects in heteroepitaxial β-Ga2O3 films

Saadatkia, P.; Agarwal, S.; Hernandez, A.; Reed, E.; Brackenbury, I. D.; Codding, C. L.; Liedke, M. O.; Butterling, M.; Wagner, A.; Selim, F. A.;

Originally published:

October 2020

Physical Review Materials 4(2020), 104602

DOI: https://doi.org/10.1103/PhysRevMaterials.4.104602

Perma-Link to Publication Repository of HZDR:

https://www.hzdr.de/publications/Publ-31609

Release of the secondary publication
on the basis of the German Copyright Law § 38 Section 4.

Point and extended defects in heteroepitaxial β-Ga_2O_3 films

P. Saadatkia,[1,2] S. Agarwal,[1,2] A. Hernandez,[1,2] E. Reed,[2] I. D. Brackenbury,[2] C. L. Codding,[1,2] M. O. Liedke,[3] M. Butterling,[3] A. Wagner,[3] F. A. Selim[1,2*]

[1] Center for Photochemical Sciences, Bowling Green State University, Bowling Green, OH 43403, USA.

[2] Department of Physics and Astronomy, Bowling Green State University, Bowling Green, OH 43403, USA.

[3] Institute of Radiation Physics, Helmholtz-Zentrum Dresden-Rossendorf, Bautzner Landstr. 400, 01328 Dresden, Germany.

*faselim@bgsu.edu, +1(419) 372-9956

ABSTRACT

Ga_2O_3 is emerging as an excellent potential semiconductor for high power and optoelectronic devices. However, the successful development of Ga_2O_3 in a wide range of applications requires a full understanding of the role and nature of its point and extended defects. In this work, high quality epitaxial Ga_2O_3 films were grown on sapphire substrates by metal-organic chemical vapor deposition and fully characterized in terms of structural, optical, and electrical properties. Then defects in the films were investigated by a combination of depth-resolved Doppler broadening and lifetime of positron annihilation spectroscopies and thermally stimulated emission (TSE). Positron annihilation techniques can provide information about the nature and concentration of defects in the films, while TSE reveals the energy level of defects in the bandgap. Despite very good structural properties, the films exhibit short positron diffusion length, which is an indication of high defect density and long positron lifetime, a sign for the formation of Ga vacancy related defects and large vacancy clusters. These defects act as deep and shallow traps for charge carriers as revealed from TSE, which explains the reason behind the difficulty of developing conductive

Ga_2O_3 films on non-native substrates. Positron lifetime measurements also show nonuniform distribution of vacancy clusters throughout the film depth. Further, the work investigates the modification of defect nature and properties through thermal treatment in various environments. It demonstrates the sensitivity of Ga_2O_3 microstructures to the growth and thermal treatment environments and the significant effect of modifying defect structure on the bandgap and optical and electrical properties of Ga_2O_3.

I. INTRODUCTION

β-Ga_2O_3 has recently attracted a great deal of interest in optoelectronics and high-power devices due to its wide bandgap of 4.5- 4.9 eV [1]. It has potential applications in deep UV photodetectors [2,3], short-wavelength light-emitting diodes [4], transparent conducting oxides [5,6], high-power devices [7], and solar blind photodiodes [8]. Compared to other wide bandgap materials like SiC and GaN, it has a higher Baliga figure of merit and breakdown field, which makes it an excellent candidate for high power devices [7]. Full understanding of point and extended defects in Ga_2O_3 is crucial for its further development for devices. Moreover, our recent work revealed that chemical manipulation of defects can induce both electron and hole conduction in β-Ga_2O_3 single crystals [9].

There are five polymorphs of Ga_2O_3 α, β, γ, δ, ε; β phase is the most stable and the only one that can be grown from the melt growth techniques including floating-zone (FZ), edge-defined film-fed growth, and Czochralski approaches which allows the possibility of mass production of large-size single crystals substrates [7,10-15]. β-Ga_2O_3 crystallizes in monoclinic structure with lattice parameters of a = 12.2 Å, b = 3.0 Å and c = 5.8 Å [7]. Substrate lattice and growth temperature play an important role in the creation of different phases in Ga_2O_3 films. The formation of β phase Ga_2O_3 occurs at high temperatures for both homo [16] and hetero-epitaxial growth [7]. Different

methods have been used for the growth of thin film Ga_2O_3 such as molecular beam epitaxy (MBE) [3,17-19], halide vapor phase epitaxy (HVPE) [20-22], pulsed laser deposition (PLD) [23], mist chemical vapor deposition (mist-CVD) [24-25] and metal-organic chemical vapor deposition (MOCVD) [26-29]. Among these techniques, MOCVD is expected to produce β-Ga_2O_3 films of enhanced crystalline quality due to the thermodynamically favorable growth process in this technique [26]. Also, MOCVD has a higher deposition rate than most of growth techniques, excellent compositional control, uniform coverage and is easy for large-scale production [30-31]. β-Ga_2O_3 has been deposited on different substrates including native substrates using the MOCVD technique; p-type Si substrate was used to deposit Ga_2O_3 films by Kim et al. [27] at temperatures of 500-600 ^{o}C, which showed an increase in surface roughness of the films at increased temperature. Mi et al. [32] grew epitaxial β-Ga_2O_3 films on the $MgAl_2O_4$ substrate at different temperatures (550-700 ^{o}C). According to their results, 650 ^{o}C substrate temperature resulted in the best crystallinity of β-Ga_2O_3 films. Differently oriented Al_2O_3 and GaAs were also used as substrates for epitaxial growth of β-Ga_2O_3 [28].

Although β-Ga_2O_3 is the most well studied phase of Ga_2O_3, little is understood about its native defects. In this work, we investigate defects in epitaxial β-Ga_2O_3 films grown by the MOCVD method employing various characterization techniques. Al_2O_3 (0001) (C-sapphire) was used as a substrate and the grown films were annealed in different environments to populate different types of defects in Ga_2O_3. The Structural characteristics of the films were analyzed by X-ray diffraction (XRD) and atomic force microscopy (AFM) techniques. The optical and electrical properties of the films were determined by UV-Vis spectroscopy and Hall Effect measurements. Atomic force microscopy (AFM) was also applied to study the surface morphology of the films before and after annealing. Then, thermal stimulated emission (TSE) in conjunction with depth-resolved positron

annihilation lifetime spectroscopy (PALS) and Doppler broadening spectroscopy (DBS) were used to study point defects in the films.

II. EXPERIMENTAL DETAILS

A. Fabrication of Epitaxial Ga_2O_3 Films

One-side polished sapphire substrates of about 5 cm diameter with C orientation were used to grow Ga_2O_3 by the MOCVD technique. Substrates were cleaned in organic solvents, then dried by compressed nitrogen before loading them into the reactor. The epitaxial growth of Ga_2O_3 took place in a vertical geometry cold wall reactor (Agnitron Inc.) for 1.5 hours. Trimethylgallium (TMGa) ($Ga(CH_3)_3$) was used as a metal-organic source and kept in a bubbler set at a temperature of -10 ^oC and pressure of 900 Torr. TMGa vapor was introduced to the reactor using high purity Ar (99.999%) that acts as a carrier gas. Pure oxygen gas (99.999%) was used as a precursor for oxygen. The substrate was rotating at 800 rpm during the growth process to allow better coverage and produce uniform films. The substrate temperature was 740 ^oC during the growth and the chamber pressure was kept at 65 Torr. To populate different types of point defects, the Ga_2O_3 films grown on sapphire were cut to 1cm x1cm pieces and annealed in two different environments, either Ar flow or ambient air for one hour at 1000 ^oC.

B. Structural and Optical Characterization

The structural properties of the films were analyzed by X-ray diffraction (XRD); their XRD patterns were recorded using a Rigaku diffractometer [33]. Atomic Force Microscopy (AFM) measurements were performed to investigate the surface morphology of the films. A double beam UV-Vis Perkin Elmer spectrometer was used to record the optical absorption spectra from 190 nm to 1100 nm, and the optical band gap of Ga_2O_3 films was then calculated from the absorption

spectra using Tau equation [34-35]. The electrical transport properties of the films were measured using Hall-effect system in Van der Pauw configuration described elsewhere [36].

C. Defect Spectroscopy

In order to identify point defects in the films and calculate their activation energies, TSE and positron annihilation spectroscopies were used. TSE measurements were carried out using a spectrometer that was built in house by one of the authors. The details of the spectrometer and the methods of analysis are described elsewhere [37-39]. Samples were irradiated with UV light using a pulsed xenon lamp for 30 minutes at liquid nitrogen (77 K) and ramp-up to 673 K. The measurements were carried out at two heating rates of 60 K/min and 120 K/min. Depth-resolved positron annihilation spectroscopy (PAS) was used to study vacancy type defects in the as-grown and annealed Ga_2O_3 thin films. The PAS measurements were performed at the positron facility in the Helmholtz-Zentrum Dresden-Rossendorf (HZDR) in Dresden, Germany [40]. The Slow-Positron System of Rossendorf (SPONSOR) beamline featuring a continuous DC monoenergetic beam was used to perform Doppler broadening spectroscopy (DBS) with incident positron energies in the range of 0.04-17 keV [40,41]. At each energy, the characteristic 511 keV gamma was recorded via a high purity Ge detector with an energy resolution in the order of 1.09 ± 0.01 keV. The line shape and wing parameters, namely, 'S' and 'W', were constructed from the experimental data by measuring the relative change in the characteristic 511keV peak induced due to the Doppler shift of low-momentum valence electrons and high-momentum core electrons respectively. Details about DBS spectroscopic measurements and analysis can be found elsewhere [42-43]. In addition, the Electron Linac for beams with high Brilliance and low Emittance (ELBE) positron facility also at the HZDR, Germany features depth-resolved PALS capabilities at the

Monoenergetic Positron Spectroscopy (MePS) beamline with a positron flux of ~10^6/s. PALS measurements were performed for incident positron energies between 2-16 keV and more than 5 million counts were collected at each beam energy for good statistics [40]. The lifetime spectra were acquired as time derivative of the positron decay events and the resolution function was determined to be < 230 ps. The resultant spectra were deconvoluted into individual lifetime components using the PALSfit software [44].

III. RESULTS AND DISCUSSION

A. Structural Characterization

FIG. 1 shows the XRD patterns of Ga_2O_3 films grown on a sapphire substrate (0001) at a temperature of 740 °C and pressure of 65 Torr. The peak corresponding to sapphire (around 2θ ~ 42°) was removed from the XRD pattern. The figure shows four peaks located at 2θ ~ 19.30°, 38.70°, 59.40°, 82.40° corresponding to β-Ga_2O_3 $(\bar{2}01)$, $(\bar{4}02)$, $(\bar{6}03)$, and $(\bar{8}04)$. The XRD pattern indicates that the films are single phase of β-Ga_2O_3 and epitaxial with single orientation along $[\bar{2}01]$ direction. Growth temperature is a key factor to control the crystal structure of Ga_2O_3 and produce epitaxial films. There are previous reports on obtaining epitaxial single phase β-Ga_2O_3 films at different temperatures and pressures. Besides temperature and pressure, other factors such as flow rate and substrate orientation may affect the crystallinity and epitaxial nature of the films. In this work, high quality epitaxial β-Ga_2O_3 films were obtained at 740 °C and 65 Torr while Lv et al. [45] reported 650 °C as the best temperature for epitaxial growth of β-Ga_2O_3 films on a sapphire substrate using growth pressure of 20 Torr. They showed that by increasing the temperature above 650 °C, the film's structure changed to polycrystal whereas, in the current study, temperatures below 740 °C result in polycrystalline films, however, the growth pressure was 65 Torr. Similarly, Boschi et al. [46] reported that 715 °C is the minimum temperature required to

obtain epitaxial β-Ga_2O_3 films and 650ºC resulted in the formation of ε-Ga_2O_3 films at 100 mbar growth pressure.

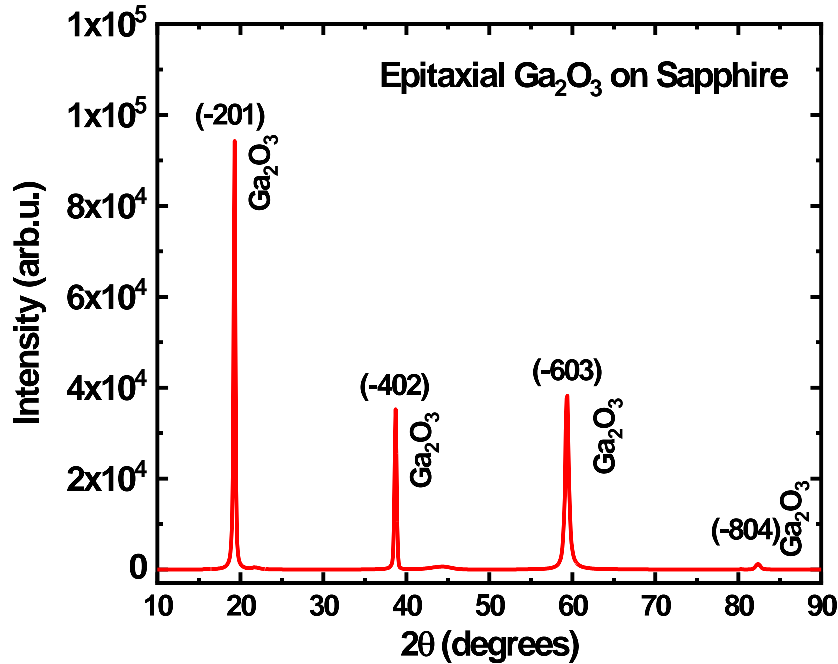

FIG. 1. XRD pattern of Ga_2O_3 film grown on a sapphire substrate (0001) at a growth temperature of 740 ºC.

As mentioned earlier, we used two different environments (Ar and air) to anneal β-Ga_2O_3 films after MOCVD growth. The morphology of the as-grown and annealed films were then investigated by AFM measurements. FIGs. 2 (a), (b), and (c) show how the surface of the film changed after annealing in various environments. The root-mean-square (RMS) roughness values of the as-grown and Ar- and air-annealed films are 0.486 nm, 16.2 nm, and 5.62 nm, respectively. As can be seen from the figures, the surface of as-grown β-Ga_2O_3 film is flat and uniform, while annealing in different environments prominently increased the roughness of the film, especially after Ar-anneal. The smooth surface of the as-grown film from AFM measurements and the very intense and narrow diffraction peaks observed in XRD measurements confirm the high quality of the films

grown by MOCVD. The FWHM of 0.27°, 0.30°, 0.56°, 0.70° were calculated for (-201), (-402), (-603), and (-804) respectively.

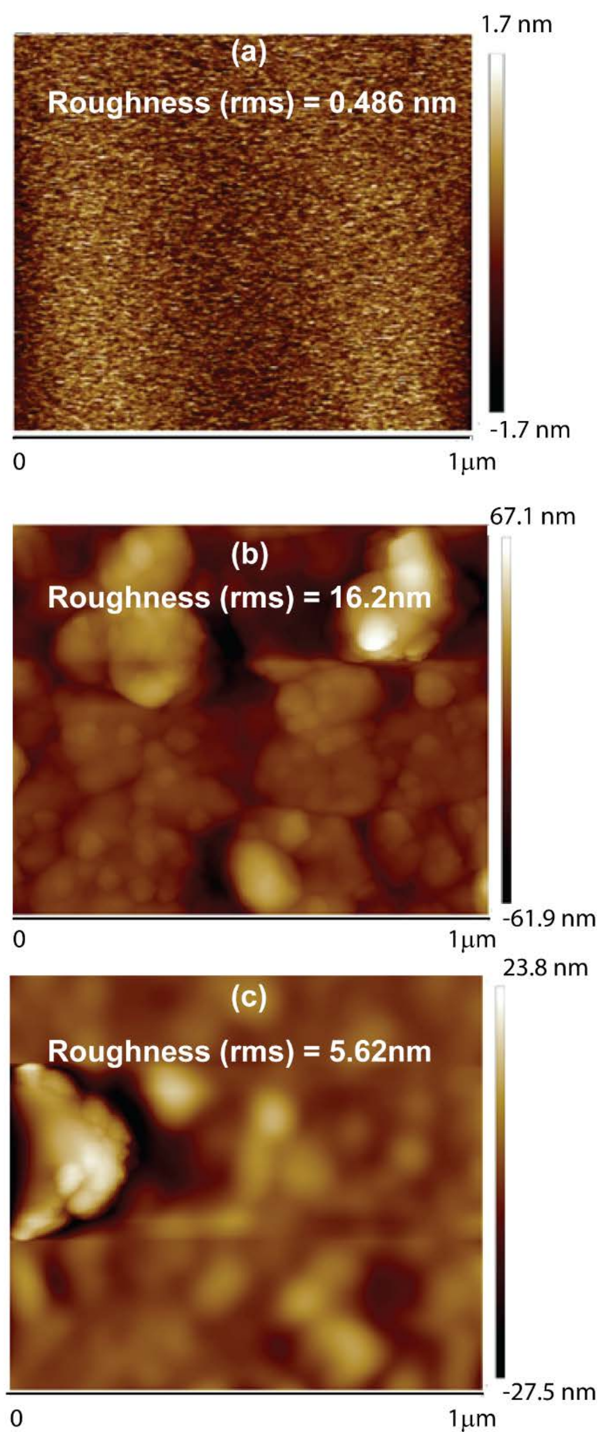

FIG. 2. AFM images of Ga_2O_3 films grown by MOCVD on a sapphire substrate (0001) at a growth temperature of 740 °C: (a) as-grown, (b) annealed in Ar flow, (c) annealed in O_2 flow.

B. Optical properties of Ga_2O_3 films

FIG. 3 (a) shows the optical absorption spectrum in the range of 190-1100 nm for the as-grown and annealed β-Ga_2O_3 films grown on sapphire by MOCVD technique. The as-grown, Ar-annealed and air-annealed samples showed a strong absorption peak below 275 nm (4.5 eV). The Ar-annealed sample shows much higher absorption starting from 275 nm through the visible region and near-infrared (NIR) region compared to other samples in addition to a shift in the optical band gap, this can be seen from the sample color which turned bluish after annealing.

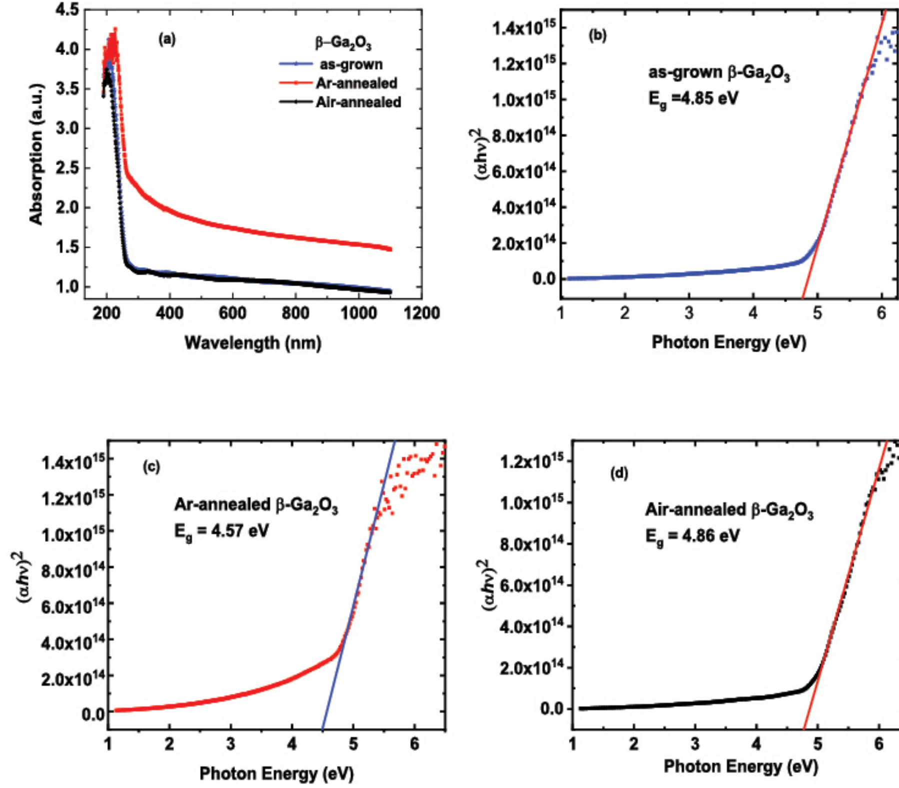

FIG. 3. Optical Measurements. (a) Room-temperature optical absorbance spectra of as-grown, Ar-annealed, and air-annealed films, (b) Plot of $(\alpha h\nu)^2$ as a function of photon energy for the as-grown β-Ga_2O_3 film. α is the absorption coefficient, (c) Plot of $(\alpha h\nu)^2$ as a function of photon energy for the Ar-annealed β-Ga_2O_3 film, (d) Plot of $(\alpha h\nu)^2$ as a function of photon energy for the air-annealed β-Ga_2O_3 film.

The optical band gap energy was calculated from the absorption coefficient (α) given by $\alpha = 2.303\ (\frac{A}{d})$ Where A is the absorbance that is measured by UV-Vis spectrometer and d is the film thickness. Using Tauc equation [47-49] for direct bandgap materials, the relation between absorption coefficient and photon energy can be written as $\alpha h\nu \propto (h\nu - E_g)^{1/2}$, where α is the absorption coefficient and E_g is the bandgap. After plotting $(\alpha h\nu)^2$ versus photon energy hν, bandgap energy E_g can be estimated by extrapolation of the linear part to αhν=0. The optical band gap energy of 4.85 eV, 4.57 eV, and 4.86 eV was calculated for as-grown, Ar-annealed, and air-annealed β-Ga_2O_3 films, respectively as shown in FIGs. 3 (b), (c), and (d).

C. Electrical properties of Ga_2O_3 films

Hall effect measurements were carried out on as-grown and annealed β-Ga_2O_3 films using Van der Pauw configuration and the sheet resistance and sheet number (Sheet Carrier Concentration) of the films are presented in Table I. The sheet resistance and sheet number of the as-grown films are $8.13\text{x}10^8$ Ω /cm^2 and $7.42\text{x}10^6$ cm^{-2}, which is consistent with high resistive undoped films and indicates the absence of background conductivity. After annealing in air, the sample became too resistive to measure its electrical properties, which is similar to the results attained by Galazka et al. [50]. However, annealing in Ar flow slightly decreases the sheet resistance to $1.88\text{x}10^8$ Ω /cm^2. All samples were transparent even after annealing except the samples that were annealed in Ar, which changed to blue color and has the lowest sheet resistance and highest sheet number. Comparing with the growth of β-Ga_2O_3 single crystals under different conditions by Galazka et al. [50], the samples that were grown in CO_2 + Ar environment, have a blue color and show higher conductivity than transparent samples, same as the Ar-annealed β-Ga_2O_3 films in this study.

TABLE I. Hall effect measurements for as-grown and annealed β-Ga_2O_3 thin films grown on sapphire by MOCVD technique.

Samples	Sheet resistance (Ω/cm^2)	Sheet number (cm^{-2}) (Sheet Carrier Concentration)
Ga_2O_3- as-grown	$8.13x10^8$	$7.42x10^6$
Ga_2O_3- Ar-annealed	$1.88x10^8$	$9.50x10^6$
Ga_2O_3- air-annealed	Too resistive	Too resistive

D. Defect studies

Positron annihilation spectroscopy (PAS) has been established as a powerful technique for identifying vacancy type defects in oxides and semiconductors as it can provide information about the type and density of point defects in the lattice [42,43, 51-55]. In this work, depth-resolved PALS and DBS measurements in conjunction with TSE spectroscopy were utilized to investigate point defects in hetero-epitaxial β-Ga_2O_3 thin films and understand the effect of different annealing environments on the defect structures and the optical and electrical properties of the films.

1. TSE measurements and trap levels calculations

We have established the use of TSE or thermal stimulated luminescence spectroscopy technique for the calculations of activation energy of defects in a wide range of oxides in different forms of nanostructures, transparent ceramics and single crystals. [56-59]. In this work, TSE measurements were carried out on as-grown and annealed β-Ga_2O_3 thin films, and thermal activation energy of shallow and deep level electronic defects was calculated. Figure 4 (a) shows TSE curve as a function of temperature for as-grown, Ar-annealed and Air-annealed samples. As can be seen from the figure, all films show a peak at low temperature, TSE intensity decreases after annealing in air and increases after annealing in argon flow. The activation energy of the trap associated with these

peaks was calculated using the initial-rise method [60] and summarized in TABLE II. It was found to be 0.027 eV for as-grown films and changed to 0.024 eV and 0.020 eV after annealing in Ar- and air-flow, respectively. Although all films did not show much conductivity, the Ar-annealed sample was more conductive than as-grown and air annealed sample was too resistive to be measured with our system. Because this change of conductivity is associated with the corresponding change in the intensity of TSE peaks (FIG. 4 (a)), we expect that these TSE peaks at low temperature are related to defects that act as shallow donors and induce low conductivity in the films. These defects are most likely related to oxygen vacancy complex defects, which have been filled after annealing in air and result in reducing the TSE intensity and conductivity of the films. FIG. 4 (b) presents high temperature TSE glow curves for as-grown and air-annealed β-Ga_2O_3 thin films. It shows two broad emission peaks for both films at high temperatures. No emission was detected after Ar flow. TSE peaks are reduced after annealing the sample in air, which may be due to the decrease of luminescence center concentrations.

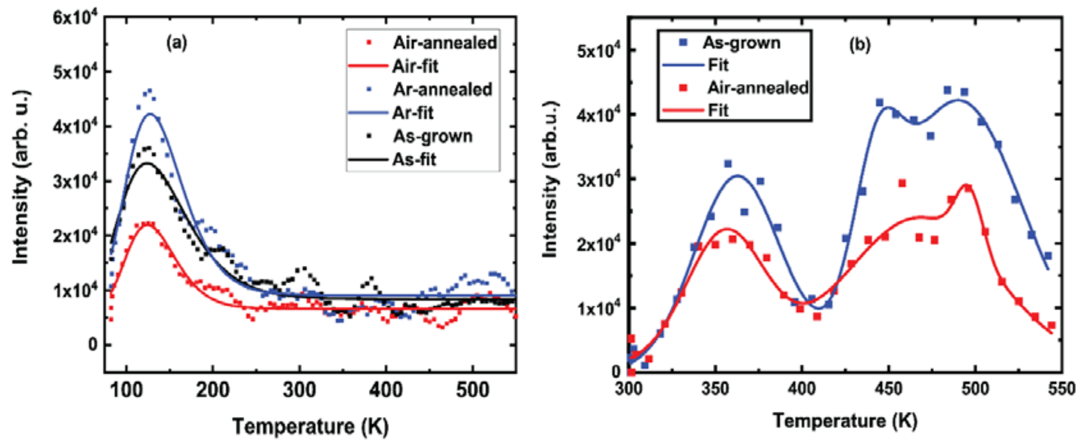

Figure 4. TSE measurements on as-grown and annealed samples. (a) Low temperature TSE glow curve for as-grown and annealed β-Ga_2O_3 thin films. The measurements were carried out at 60 K/min, (b) High temperature TSE glow curves for as-grown and air-annealed β-Ga_2O_3 thin films. The measurements were carried out at 120 K/min. No emission at high temperatures appeared after Ar anneal. The solid lines represent the Gaussian multi-peaks fits of the experimental data (symbols).

TABLE II. Thermal activation energies of shallow level defects in as-grown and annealed β-Ga_2O_3 thin films. Initial rise method was used for calculating activation energies. The heating rate was 60 K/min.

Samples	**Temperature associated with maximum intensity (K)**	**Activation energy (eV)**
As-grown	127	0.027±0.003
Ar-annealed	126	0.024±0.003
Air-annealed	126	0.020±0.002

The thermal activation energies of the trap levels associated with these peaks for as-grown and air-annealed films are summarized in TABLE III. For as-grown samples, the activation energies are 0.707 eV and 0.722 eV associated with 362.77 K and 479.70 K. Annealing in the air not only decreased the intensity of the TSE peak but also changed the defect activation energies to 0.540 eV and 0.431 eV. There are some reports that investigated deep level defects in β-Ga_2O_3 [60-65] bulk single crystals and it is useful to compare these reports with the current measurements. Recently, Ingebrigtsen et al. [65] reported two defect levels very close to each other located at 0.78 eV and 0.75 eV. They believe that Fe_{Ga} and a native defect or defect complex are responsible for these deep level defects, respectively. Several defect levels associated with oxygen and gallium vacancies have been reported by Gao et al. [64] using deep level transient spectroscopy. Islam et al. [60] also used TSE spectroscopy to study trap levels in undoped and doped β-Ga_2O_3 single crystals. In this previous work, the deep trap level with 0.751 eV activation energy reported for undoped β-Ga_2O_3 associated with 458.15 K is close to the second peak we observe in the current as-grown heteroepitaxial film.

TABLE III. Thermal activation energies of deep-level defects in as-grown and air-annealed β-Ga_2O_3 thin films. Initial rise method was used for calculating activation energy. The heating rate was 120 K/min.

Samples	**Temperature associated with maximum intensity (K)**	**Activation energy (eV)**
As-grown	363	0.707±0.029
As-grown	480	0.722±0.027
Air-annealed	360	0.540±0.031
Air-annealed	472	0.431±0.034

Assuming that the traps in the as-grown sample are associated with V_O-V_{Ga} complexes, the oxygen vacancies in some of these complexes can be filled after air-anneal leading to a decrease in TSE. For Ar-annealed sample, no emission associated with deep traps at high temperatures was observed. One possibility is that the structure of defects has changed and they became inactive traps for charge carriers, or they might not be an active luminescence center anymore. While TSE measurements provide important information about the energy level of both shallow and deep defect centers in the bandgap, it cannot reveal the nature of these trapping defects. Only some assumptions can be made about their nature from combining annealing with TSE results. On the contrary, PAS cannot provide information about the energy levels of defects or their activation energies, however it is powerful technique to reveal the nature and charge state of defects in semiconductors and oxides as well as their concentration [51-55].

2. Positron annihilation spectroscopy

To understand the nature of trapping defects in Ga_2O_3 films, we apply depth-resolved positron annihilation lifetime spectroscopy (PALS) and Doppler broadening spectroscopy (DBS). FIG. 5 (a) presents S and W parameters as a function of incident positron energy and mean implantation depth for as-grown and annealed β-Ga_2O_3 thin films. S parameter (shape parameter) represents the annihilation fraction of positrons with valence electrons, which is defined as the number of annihilation events in the center of the spectrum, the low electron momentum part, divided by the total number of events in the peak. W parameter (wing parameter) represents the annihilation fraction of positrons with core electrons, defined as the number of annihilation events in the wings of the 511 keV peak, the high electron momentum part, divided by the total number of counts in the peak [42-43]. Positron trapping at defects leads to an increase in S parameter and a decrease in W parameter as the positron wave function overlaps more with valence electrons in the vacancy region. The high S value at the beginning of S-E curve in Fig. 5a is common in DBS due to positronium formation at the surface. Ar-annealed sample exhibits a very high S parameter throughout the film thickness indicating high content of defects. S values for as-grown and air-annealed films are very close throughout the thickness of the film except at the first 70 nm.

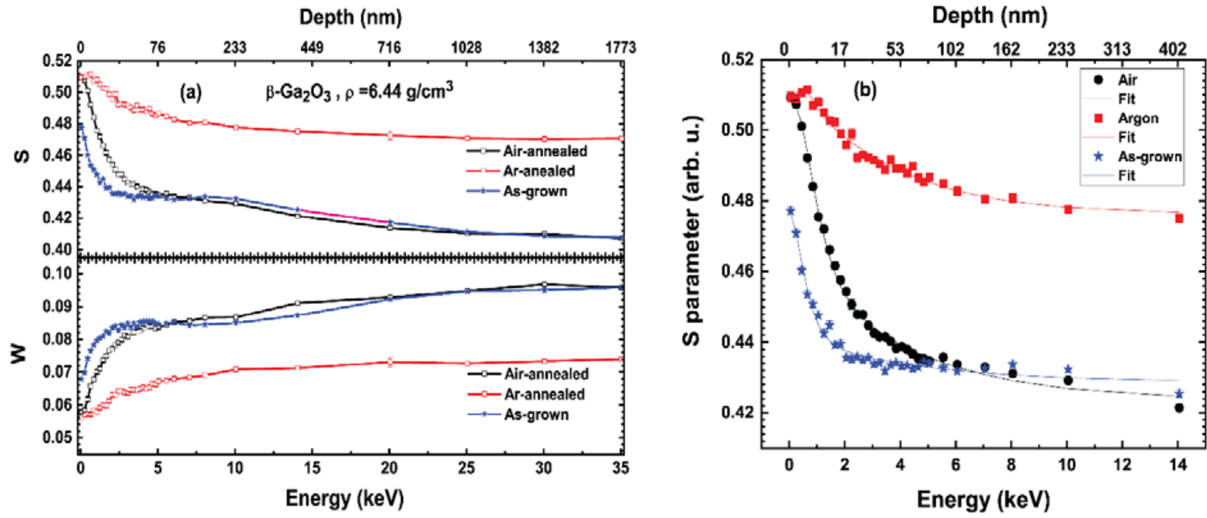

FIG 5. Results from DBS measurements for as-grown and annealed films. (a) S and W parameters as a function of positron beam energy and mean positron implantation depth for as-grown, Ar-annealed, and air-annealed β-Ga_2O_3 thin films grown on sapphire by MOCVD technique, (b) Fitting of S(E) profiles using VEPFIT.

The fitting of S(E) profiles using VEPFIT code [66] is presented in FIG. 5 (b) to estimate the respective positron diffusion lengths (L_+) for each sample [67]. L_+ is another direct indicator for the amount of defects in the structure as point defects trap and scatter positrons reducing their diffusion lengths. The VEPFIT program employs a fitting regime based on the solution of time-averaged positron density equation. For the fitting, the density of β-Ga_2O_3 was taken as ~6.44 g/cm^3 and the annihilation rate was assumed to be ~5.68 ns^{-1} based on the reported bulk lifetime value of 176 ps [68-69]. The input model used for the analysis was model '4' [67] which applied different layered structures of defects. To avoid any contribution from the substrate, the fitting was carried out in the range 0-14 keV. The fitting required determination of two layers (layer-1: surface, layer-2: near-surface region and bulk of the film) for each sample. For air-annealed, the

width of layer-1 was determined to be ~28 nm and the positron diffusion length was found to be around 7 (0.2) nm. Similarly, for Ar-annealed and as-grown the surface layer atop of the films were found to be ~ 15 and 11 nm wide and the effective positron diffusion length (L_+) values were found to be around 4 (0.4) and 2 (0.5) nm. In contrast, for the bulk-region of films, a low L_+ of ~ 60 (1) nm was estimated for the Ar-annealed sample compared to L_+= 84 (2) nm for the air-annealed and 89 (4) nm for as-grown samples. The diffusion length (L_+) in all films is much shorter than the 220-250 nm range, the typical bulk diffusion length commonly observed for most semiconductors and oxides [42-43] indicating high level of defects in all films.

We also performed depth-resolved PALS on Ar- and air- annealed Ga_2O_3 films covering positron implantation energies from 2 to 16 keV corresponding to 0 to ~500 nm depth in the films. PALS measurements give invaluable information on the size of vacancies and vacancy clusters in oxides and semiconductors. At each beam energy, the positron lifetime spectrum was recorded and fitted using PALSfit code [44]. Two lifetime components were resolved at each depth, their values and intensities are presented in FIG. 6 (a) and (b). An additional third component with lifetime values in the range of 1-2 nm was also obtained and ignored due to its negligible intensity. This component is often observed in this spectrometer measurements; it is due to positron backscattering and contribution from annihilation at the surface. The positron lifetime values, which reflect the size of positron tapping sites, show a significant change as a function of depth (Fig. 6(a)). Similarly, their corresponding intensities, which are indicative of the relative defect density, are also quite different throughout the depth (Fig. 6(b)). Thus, the measurements reveal nonuniform distribution in the size and density of the vacancy clusters throughout the film depth. The values of the two lifetime components at all depths are much larger than τ_B, the positron bulk lifetime of Ga_2O_3, which was reported to be around 176 ps [68-69]. This indicates complete

positron trapping at defects and that no positron annihilation took place in the bulk due to a high level of defects, which is consistent with the short positron diffusion lengths discussed above. Table IV compares the lifetime components in the bulk of the films around 102 nm depth where the largest lifetime components were obsereved. In air annealed sample, the first lifetime component τ_1 (~205 ps) is much longer than the bulk lifetime in Ga2O3 and is in the range of the lifetime values of cation vacancies in most oxides. Because of that and because positron cannot be trapped in oxygen vacancies due to their positive charges, this lifetime component is expected to be associated with Ga vacancies. The second lifetime τ_2 (~417 ps) is quite high, indicating the presence of large extended vacancy clusters which could be vacancies in close proximity or small voids [42,70]. Ar annealing had led to a significant increase in τ_1 and τ_2, signifying the increase of the cluster size. Annealing in Ar provides a neutral atmosphere and most likely led to the formation of clusters containing both anion and cation vacancies. In fact, these PALS measurements show that the complete suppression of TSE after Ar- annealing is a result of the modification of defect structures and the associated change in their charge states. These defects are responsible for the blue coloration of Ga_2O_3 discussed above and the decrease in the optical band gap from 4.85 to 4.57 eV. Unfortunately, there was no as-grown sample available for PALS measurements, however DBS measurements in FIG. 5 (a) show close S(E) and W(E) curves in as-grown and air-annealed films throughout the depth. This indicates similar or close defect structure in the two films. Accordingly, it is reasonable to assume that the PALS measurements of air-annealed film give a good representation for the dominant defect structure in as-grown films.

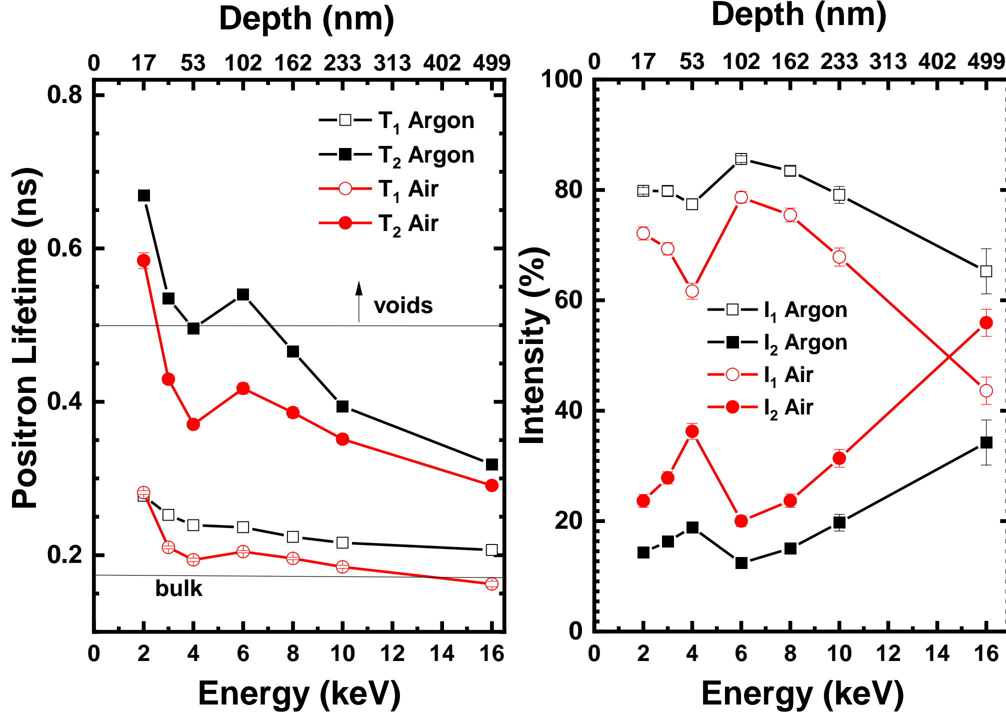

FIG. 6. Positron lifetime components and corresponding intensities as a function of positron beam energy and mean positron implantation depth for Ar- and air-annealed β-Ga_2O_3 thin films. The reported bulk and void lifetimes are marked on the graphs. The graphs reveal th presence of large vacancy clusters and indicate nonuniform distribution in their size and density

TABLE IV. Lifetime components and corresponding intensities at E=6 keV (102 nm) for Ar-annealed, and air-annealed β-Ga_2O_3 thin films grown on sapphire by MOCVD technique. The average lifetime value is also presented.

Samples	τ_1 (ns)	I_1	τ_2 (ns)	I_2	τ_{avg} (ns)
Ga_2O_3-Ar	0.236±0.001	85.58	0.540±0.011	12.41	0.344±0.011
Ga_2O_3-air	0.205±0.001	78.67	0.417±0.007	20.00	0.287±0.013

IV. CONCLUSIONS

High quality β-Ga_2O_3 single crystal thin films were grown by MOCVD on sapphire substrates in order to study point defects in heteroepitaxial Ga_2O_3 films. PAS identified high level of Ga vacancy

related defects and revealed the presence of unusual large vacancy clusters in the films despite of the good structural quality of the films revealed from XRD measurements. By studying TSE from the films, point defects were shown to occupy both shallow and deep levels in the bandgap. However, no significant background conductivity was observed in conjunction with the shallow levels. This high level of point defects revealed from PAS measurements explains the reason behind the common difficulty of achieving good conductivity in Ga_2O_3 on non-native substrates even when doped with potential donors. Annealing in different atmospheres populate different defect structures revealing the sensitivity of Ga_2O_3 lattice to the growth and treatment environments. Annealing in Ar atmosphere led to the formation of very large vacancy clusters modifying their defect structure and charge state. These large vacancy clusters are responsible for the blue coloration and the significant shift in the band gap demonstrating the large effect of point-defects on the optoelectronic properties of Ga_2O_3.

ACKNOWLEDGEMENTS

Research was supported as part of FUTURE (Fundamental Understanding of Transport Under Reactor Extremes), an Energy Frontier Research Center funded by the U.S. Department of Energy (DOE), Office of Science, Basic Energy Sciences (BES) (analysis of positron annihilation spectroscopy data) and by the National Science Foundation (NSF) under Award # DMR-2005064 (collection of PAS data, collection and analysis of TSE data). A part of this research was carried out at the ELBE facility at the Helmholtz-Zentrum Dresden-Rossendorf (HZDR) e. V., a member of the Helmholtz Association. We would like to thank the facility staff for assistance.

REFERENCES

1. Tippins, H. Optical absorption and photoconductivity in the band edge of β−Ga_2O_3. *Phys. Rev.* **1965***, 140*, A316.

2. Kokubun, Y.; Miura, K.; Endo, F.; Nakagomi, S. Sol-gel prepared β−Ga_2O_3 thin films for ultraviolet photodetectors. *Appl. Phys. Lett.* **2007***, 90*, 031912.

3. Oshima, T.; Okuno, T.; Fujita, S. Ga_2O_3 thin film growth on c-plane sapphire substrates by molecular beam epitaxy for deep-ultraviolet photodetectors. *Jpn. J. Appl. Phys.* **2007***, 46*, 7217.

4. Santos, N.; Rodrigues, J.; Fernandes, A.; Alves, L.; Alves, E.; Costa, F.; Monteiro, T. Optical properties of LFZ grown β-Ga_2O_3: Eu^{3+} fibres. *Appl. Surf. Sci.* **2012***, 258*, 9157-9161.

5. Ueda, N.; Hosono, H.; Waseda, R.; Kawazoe, H. Anisotropy of electrical and optical properties in β-Ga_2O_3 single crystals. *Appl. Phys. Lett.* **1997***, 71*, 933-935.

6. Passlack, M.; Schubert, E.; Hobson, W.; Hong, M.; Moriya, N.; Chu, S.; Konstadinidis, K.; Mannaerts, J.; Schnoes, M.; Zydzik, G. Ga_2O_3 films for electronic and optoelectronic applications. *J. Appl. Phys.* **1995***, 77*, 686-693.

7. Higashiwaki, M.; Sasaki, K.; Murakami, H.; Kumagai, Y.; Koukitu, A.; Kuramata, A.; Masui, T.; Yamakoshi, S. Recent progress in Ga_2O_3 power devices. *Semicond. Sci. Tech.* **2016***, 31*, 034001.

8. Feng, P.; Zhang, J.; Li, Q.; Wang, T. Individual β-Ga_2O_3 nanowires as solar-blind photodetectors. *Appl. Phys. Lett.* **2006***, 88*, 153107.

9. Islam, M.M.; Liedke, M.O.; Winarski, D.; Butterling, M.; Wagner, A.; Hosemann, P.; Wang, Y.; Uberuaga, B.; and Selim, F.A. Chemical manipulation of hydrogen induced high p-type and n-type conductivity in Ga2O3. *Scientific reports* **2020**, *10*(1).

10. Sasaki, K.; Higashiwaki, M.; Kuramata, A.; Masui, T.; Yamakoshi, S. Si-ion implantation doping in β-Ga_2O_3 and its application to fabrication of low-resistance ohmic contacts. *Appl. Phys. Express* **2013***, 6*, 086502.

11. Ueda, N.; Hosono, H.; Waseda, R.; Kawazoe, H. Synthesis and control of conductivity of ultraviolet transmitting β-Ga_2O_3 single crystals. *Appl. Phys. Lett.* **1997***, 70*, 3561-3563.

12. Suzuki, N.; Ohira, S.; Tanaka, M.; Sugawara, T.; Nakajima, K.; Shishido, T. Fabrication and characterization of transparent conductive Sn-doped β-Ga_2O_3 single crystal. *Phys. Status. Solidi. C.* **2007***, 4*, 2310-2313.

13. Víllora, E. G.; Shimamura, K.; Yoshikawa, Y.; Aoki, K.; Ichinose, N. Large-size β-Ga_2O_3 single crystals and wafers. *J. Cryst. Growth* **2004***, 270*, 420-426.

14. Aida, H.; Nishiguchi, K.; Takeda, H.; Aota, N.; Sunakawa, K.; Yaguchi, Y. Growth of β-Ga_2O_3 single crystals by the edge-defined, film fed growth method. *Jpn. J. Appl. Phys.* **2008***, 47*, 8506.

15. Tomm, Y.; Reiche, P.; Klimm, D.; Fukuda, T. Czochralski grown Ga_2O_3 crystals. *J. Cryst. Growth* **2000***, 220*, 510-514.

16. Islam, M.M.; Adhikari, N.; Hernandez, A.; Janover, A.; Novak, S.; Agarwal, S.; Codding, C.L.; Snure, M.; Huang, M.; and Selim, F.A. Direct measurement of the density and energy level of compensating acceptors and their impact on the conductivity of n-type Ga2O3 films. *Journal of Applied Physics* **2020**, *127*(14), 145701

17. Víllora, E. G.; Shimamura, K.; Kitamura, K.; Aoki, K. Rf-plasma-assisted molecular-beam epitaxy of β-Ga_2O_3. *Appl. Phys. Lett.* **2006***, 88*, 031105.

18. Okumura, H.; Kita, M.; Sasaki, K.; Kuramata, A.; Higashiwaki, M.; Speck, J. S. Systematic investigation of the growth rate of β-Ga_2O_3 (010) by plasma-assisted molecular beam epitaxy. *Appl. Phys. Express* **2014***, 7*, 095501.

19. Vogt, P.; Bierwagen, O. The competing oxide and sub-oxide formation in metal-oxide molecular beam epitaxy. *Appl. Phys. Lett.* **2015***, 106*, 081910.

20. Murakami, H.; Nomura, K.; Goto, K.; Sasaki, K.; Kawara, K.; Thieu, Q. T.; Togashi, R.; Kumagai, Y.; Higashiwaki, M.; Kuramata, A. Homoepitaxial growth of β-Ga_2O_3 layers by halide vapor phase epitaxy. *Appl. Phys. Express* **2014***, 8*, 015503.

21. Nomura, K.; Goto, K.; Togashi, R.; Murakami, H.; Kumagai, Y.; Kuramata, A.; Yamakoshi, S.; Koukitu, A. Thermodynamic study of β-Ga_2O_3 growth by halide vapor phase epitaxy. *J. Cryst. Growth* **2014***, 405*, 19-22.

22. Oshima, Y.; Víllora, E. G.; Shimamura, K. Halide vapor phase epitaxy of twin-free α-Ga_2O_3 on sapphire (0001) substrates. *Appl. Phys. Express* **2015***, 8*, 055501.

23. Orita, M.; Ohta, H.; Hirano, M.; Hosono, H. Deep-ultraviolet transparent conductive β-Ga_2O_3 thin films. *Appl. Phys. Lett.* **2000***, 77*, 4166-4168.

24. Oshima, T.; Nakazono, T.; Mukai, A.; Ohtomo, A. Epitaxial growth of γ-Ga_2O_3 films by mist chemical vapor deposition. *J. Cryst. Growth* **2012***, 359*, 60-63.

25. Shinohara, D.; Fujita, S. Heteroepitaxy of corundum-structured α-Ga_2O_3 thin films on α-Al_2O_3 substrates by ultrasonic mist chemical vapor deposition. *Jpn. J. Appl. Phys.* **2008***, 47*, 7311.

26. Wagner, G.; Baldini, M.; Gogova, D.; Schmidbauer, M.; Schewski, R.; Albrecht, M.; Galazka, Z.; Klimm, D.; Fornari, R. Homoepitaxial growth of β-Ga_2O_3 layers by metal-organic vapor phase epitaxy. *Phys. Status. Solidi. A.* **2014***, 211*, 27-33.

27. Kim, H. W.; Kim, N. H. Growth of gallium oxide thin films on silicon by the metal organic chemical vapor deposition method. *Mat. Sci. Eng. B.* **2004***, 110*, 34-37.

28. Gottschalch, V.; Mergenthaler, K.; Wagner, G.; Bauer, J.; Paetzelt, H.; Sturm, C.; Teschner, U. Growth of β-Ga_2O_3 on Al_2O_3 and GaAs using metal-organic vapor-phase epitaxy. *Phys. Status. Solidi. A.* **2009***, 206*, 243-249.

29. Huang, C.; Horng, R.; Wuu, D.; Tu, L.; Kao, H. Thermal annealing effect on material characterizations of β-Ga_2O_3 epilayer grown by metal organic chemical vapor deposition. *Appl. Phys. Lett.* **2013***, 102*, 011119.

30. Shreiber, D.; Cole, M.; Enriquez, E.; Hirsch, S.; Ngo, E.; Hubbard, C.; Ivill, M.; Chen, C. Some unusual behavior of dielectric properties of $SrTiO_3$ metal organic chemical vapor deposition grown thin films. *J. Appl. Phys.* **2014***, 116*, 094101.

31. Duminica, F.; Maury, F.; Senocq, F. Atmospheric pressure MOCVD of TiO_2 thin films using various reactive gas mixtures. *Surf. Coat. Tech.* **2004***, 188*, 255-259.

32. Mi, W.; Ma, J.; Luan, C.; Xiao, H. Structural and optical properties of β-Ga 2 O 3 films deposited on $MgAl_2O_4$ (100) substrates by metal–organic chemical vapor deposition. *J. Lumin.* **2014***, 146*, 1-5.

33. Agarwal, S.; Haseman, M.S.; Leedy, K.D.; Winarski, D.J.; Saadatkia, P.; Doyle, E.; Zhang, L.; Dang, T.; Vasilyev, V.S.; and Selim, F.A. Tuning the Phase and Microstructural Properties of TiO_2 Films Through Pulsed Laser Deposition and Exploring Their Role as Buffer Layers for Conductive Films. *Journal of Electronic Materials*. **2018** *47*(4), 2271-2276.

34. Winarski, D. J.; Kreit E.; Heckman, E.M.; Flesburg, E.; Haseman, M.; Aga, R.S.; and Selim, F.A. Photoconductive ZnO Films Printed on Flexible Substrates by Inkjet and Aerosol Jet Techniques. *Journal of Electronic Materials.* **2018** *47(2),* 949-954.

35. Haseman, Micah; Saadatkia, P.; Winarski, D.J.; Selim, F.A.; Leedy, K.D.; Tetlak, S.; Look, D.C.; Anwand, W.; and Wagner, A. Effects of substrate and post-growth treatments on the microstructure and properties of ZnO thin films prepared by atomic layer deposition. *Journal of Electronic Materials.* **2016,** *45(12),* 6337-6345.

36. Saadatkia, P.; Stepanov, P.; and Selim, F.A. Photoconductivity of bulk $SrTiO_3$ single crystals at room temperature. *Materials Research Express* **2018**, *5*(1), 016202.

37. S. M. Reda, C. R. Varney, and F. A. Selim, "Radio-luminescence and absence of trapping defects in Nd-doped YAG single crystals," *Results in Physics* **2012**, *2,* 123–126.

38. Winarski, D.; Persson, C.; and Selim, F.A. Hydrogen in Insulating Y3Al5O12 strongly narrows the energy gap, *Appl. Phys. Lett.* **2014,** 105, 221110.

39. Selim, F. A.; Khamehchi, A.; Winarski, D.; and Agarwal, S. Synthesis and characterization of Ce: YAG nano-phosphors and ceramics. *Optical Materials Express* **2016,** *6*(*12)*, 3704-3715.

40. Wagner, A.; Butterling, M.; Liedke, M.O.; Potzger, K.; R. Krause-Rehberg, R. Positron annihilation lifetime and Doppler broadening spectroscopy at the ELBE facility, *AIP Conference Proceedings 1970* **2018**, 040003.

41. Winarski, D.J.; Anwand, Wagner, W.A.; Saadatkia, P.; Selim, F.A.; Allen, M.; Wenner, B. et al. Induced conductivity in sol-gel ZnO films by passivation or elimination of Zn vacancies. *AIP Advances* **2016**, *6(9)*, 095004.

42. Krause-Rehberg, R.; Leipner, H. S. Positron annihilation in semiconductors: defect studies, *Springer Science & Business Media* **1999**, *127*.

43. Tuomisto, F.; Makkonen, I. Defect identification in semiconductors with positron annihilation: experiment and theory. *Rev. Mod. Phys.* **2013***, 85*, 1583.

44. Olsen, J.V.; Kirkegaard, P.; Pedersen, N.J.; Eldrup, M.; PALSfit: a new program for the evaluation of positron lifetime spectra, *Physica status solidi C* **2007**, *4*, 4004-4006.

45. Lv, Y.; Ma, J.; Mi, W.; Luan, C.; Zhu, Z.; Xiao, H. Characterization of β-Ga_2O_3 thin films on sapphire (0001) using metal-organic chemical vapor deposition technique. *Vacuum* **2012**, *86*, 1850-1854.

46. Boschi, F.; Bosi, M.; Berzina, T.; Buffagni, E.; Ferrari, C.; Fornari, R. Hetero-epitaxy of ε-Ga_2O_3 layers by MOCVD and ALD. *J. Cryst. Growth* **2016**, *443*, 25-30.

47. Saleh, W. R.; Saeed, N. M.; Twej, W. A.; Alwan, M. Synthesis sol-gel derived highly transparent ZnO thin films for optoelectronic applications. *Adv. Mater. Phys. Chem.* **2012**, *2*, 11.

48. Xu, C.; Zhu, G.; Li, X.; Yang, Y.; Tan, S.; Sun, X.; Lincoln, C.; Smith, T. Growth and spectral analysis of ZnO nanotubes. *J. Appl. Phys.* **2008**, *103*, 094303.

49. Gupta, R.; Ghosh, K.; Patel, R.; Mishra, S.; Kahol, P. Band gap engineering of ZnO thin films by In_2O_3 incorporation. *J. Cryst. Growth* **2008**, *310*, 3019-3023.

50. Galazka, Z.; Irmscher, K.; Uecker, R.; Bertram, R.; Pietsch, M.; Kwasniewski, A.; Naumann, M.; Schulz, T.; Schewski, R.; Klimm, D. On the bulk β-Ga_2O_3 single crystals grown by the Czochralski method. *J. Cryst. Growth* **2014**, *404*, 184-191.

51. Tarun, M. C.; Selim, F. A.; McCluskey, M. D. Persistent photoconductivity in strontium titanate. *Physical Review Letters* **2013**, *111*, 187403.

52. Selim, F. A.; Weber, M. H.; Solodovnikov, D.; Lynn, K. G. Nature of native defects in ZnO. *Physical review letters* **2007**, *99*, 085502.

53. Selim, F. A.; Varney, C. R.; Tarun, M. C.; Rowe, M. C.; Collins, G. S.; McCluskey, M. D. Positron lifetime measurements of hydrogen passivation of cation vacancies in yttrium aluminum oxide garnets. *Physical Review B* **2013**, *88*, 174102.

54. Selim, F. A.; Winarski, D.; Varney, C. R.; Tarun, M. C.; Ji, J.; McCluskey, M. D. Generation and characterization of point defects in SrTiO3 and Y3Al5O12. *Results in Physics* **2015**, *5*, 28-31.

55. Weber, M. H.; F. A. Selim; D. Solodovnikov; K. G. Lynn. Defect engineering of ZnO. *Applied surface science* **2008**, 255, 68-70.

56. Agarwal, S.; Haseman, M.S.; Khamehchi, A.; Saadatkia, P.; Winarski, D.J.; Selim, F.A. Physical and optical properties of Ce: YAG nanophosphors and transparent ceramics and observation of novel luminescence phenomenon, *Optical Materials Express,* **2017** *7(3),* 1055-1065.

57. Ji, J.; Boatner, L.A.; Selim, F.A. Donor characterization in ZnO by thermally stimulated luminescence, *Appl. Phys. Lett*. **2014**, *105(4),* 041102.

58. Zhang, L.; Wu, J.; Stepanov, P.; Haseman, M.; Zhou, T.; Winarski, D.; Saadatkia, P.; et al. Defects and solarization in YAG transparent ceramics, *Photonics Research* **2019,** *7(5),* 549-557.

59. Mackay, D.T.; Varney, C.R.; Buscher, J.; Selim, F.A. Study of exciton dynamics in garnets by low temperature Thermo-luminescence, *J. Appl. Phys.* **2012**, *112(2)*, 023522.

60. Islam, M. M.; Rana, D.; Hernandez, A.; Haseman, M.; Selim, F. Study of trap levels in β-Ga_2O_3 by thermoluminescence spectroscopy. *J. Appl. Phys.* **2019***, 125*, 055701.

61. Ohba, E.; Kobayashi, T.; Kado, M.; Hoshikawa, K. Defect characterization of β-Ga2O3 single crystals grown by vertical Bridgman method. *Jpn. J. Appl. Phys.* **2016***, 55*, 1202BF.

62. Song, Y.; Zhang, H.; Lin, C.; Zhu, Y.; Li, G.; Yang, F.; Yu, D. Luminescence emission originating from nitrogen doping of β− Ga 2 O 3 nanowires. *Phys. Rev. B.* **2004**, *69*, 075304.

63. Zhang, Z.; Farzana, E.; Arehart, A.; Ringel, S. Deep level defects throughout the bandgap of (010) β-Ga_2O_3 detected by optically and thermally stimulated defect spectroscopy. *Appl. Phys. Lett.* **2016**, *108*, 052105.

64. Gao, H.; Muralidharan, S.; Pronin, N.; Karim, M. R.; White, S. M.; Asel, T.; Foster, G.; Krishnamoorthy, S.; Rajan, S.; Cao, L. R. Optical signatures of deep level defects in Ga_2O_3. *Appl. Phys. Lett.* **2018**, *112*, 242102.

65. Ingebrigtsen, M. E.; Varley, J.; Kuznetsov, A. Y.; Svensson, B. G.; Alfieri, G.; Mihaila, A.; Badstübner, U.; Vines, L. Iron and intrinsic deep level states in Ga_2O_3. *Appl. Phys. Lett.* **2018**, *112*, 042104.

66. Veen, A.; Schut, H.; Vries, J.; Hakvoort, R.A.; Ijpma, M.R. Analysis of positron profiling data by means of ‘‘VEPFIT’’. *AIP Conference Proceedings* **1991**, *218,* 171-198.

67. Agarwal, S.; Liedke, M.O.; Jones, A.C.L; Reed, E.; Kohnert, A.A.; Uberuaga, B.P.; Wang, Y.Q.; Cooper, J.; Kaoumi, D.; Li, N.; Auguste, R.; Hosemann, P.; Capolungo, L.; Edwards, D.J.; Butterling, M.; Hirschmann, E.; Wagner, A.; Selim, F.A. A new mechanism for void-cascade interaction from nondestructive depth-resolved atomic-scale measurements of ion irradiation–induced defects, *Fe. Sci. Adv*. **2020,** *6*, eaba8437.

68. Ting, W.Y.; Kitai, A.H.; Mascher, P. Crystallization phenomena in β-Ga2O3 investigated by positron annihilation spectroscopy and X-ray diffraction analysis, *Materials Science and Engineering: B* **2002,** *91*, 541-544.

69. Korhonen, E.; Tuomisto, F.; Gogova, D.; Wagner, G.; Baldini, M.; Galazka, Z.; Schewski, R.; Albrecht, M. Electrical compensation by Ga vacancies in Ga_2O_3 thin films. *Appl. Phys. Lett.* **2015***, 106*, 242103.

70. Johnson, J.M.; Chen, Z.; Varley, J.B.; Jackson, C.M.; Farzana, E.; Zhang, Z.; Arehart, A.R.; Huang, H.L.; Genc, A.; Ringel, S.A.; Van de Walle, C.G. Unusual Formation of Point-Defect Complexes in the Ultrawide-Band-Gap Semiconductor β− Ga 2 O 3. *Physical Review X* **2019**, *9*, 041027.